

Accurate Throughput Prediction of Basic Blocks on Recent Intel Microarchitectures

Andreas Abel and Jan Reineke
Saarland University
Saarland Informatics Campus
Saarbrücken, Germany
abel, reineke@cs.uni-saarland.de

ABSTRACT

Tools to predict the throughput of basic blocks on a specific microarchitecture are useful to optimize software performance and to build optimizing compilers. In recent work, several such tools have been proposed. However, the accuracy of their predictions has been shown to be relatively low.

In this paper, we identify the most important factors for these inaccuracies. To a significant degree these inaccuracies are due to elements and parameters of the pipelines of recent CPUs that are not taken into account by previous tools. A primary reason for this is that the necessary details are often undocumented. In this paper, we build more precise models of relevant components by reverse engineering using microbenchmarks. Based on these models, we develop a simulator for predicting the throughput of basic blocks. In addition to predicting the throughput, our simulator also provides insights into how the code is executed.

Our tool supports all Intel Core microarchitecture generations released in the last decade. We evaluate it on an improved version of the BHive benchmark suite. On many recent microarchitectures, its predictions are more accurate than the predictions of state-of-the-art tools by more than an order of magnitude.

1. INTRODUCTION

Techniques to predict the performance of software are, for example, required to build compilers, to optimize code for specific platforms, and to analyze the worst-case execution time of software in safety-critical systems. Such techniques are also useful in the area of security, where performance differences may be used for side-channel attacks.

A specific problem in this area that has received a lot of attention in recent work is to predict the performance of basic blocks, under the assumption that all memory accesses lead to cache hits. A popular performance predictor from this class is Intel's IACA [1]. It is, for example, used by the Kerncraft tool [2] to construct Roofline [3] and ECM [4] models. It has also been used by Bhattacharyya et al. [5] to build a speculative execution attack.

However, IACA is closed source, does not support recent microarchitectures, and has been discontinued by Intel in 2019. A number of alternatives were proposed in recent work, such as OSACA [6, 7], llvm-mca [8], CQA [9], Ithemal [10], and DiffTune [11].

The accuracy of the throughput predictions of previous tools compared to measurements on the actual hardware has

been shown to be relatively low; Chen et al. [12] found that the average error of previous tools compared to measurements is between 9% and 36%.

We have identified two main reasons that contribute to these discrepancies between measurements and predictions: (1) the microarchitectural models of previous tools are not detailed enough; (2) evaluations were partly based on unsuitable benchmarks, and biased and inaccurate throughput measurements. In this paper, we address both of these issues.

In the first part, we develop a pipeline model that is significantly more detailed than those of previous tools. It is applicable to all Intel Core microarchitectures released in the last decade; the differences between these microarchitectures can be captured by a small number of parameters. A challenge in building such a model is that many of the relevant properties are undocumented. We have developed microbenchmark-based techniques to reverse-engineer these properties.

Based on this model, we then implement a simulator that can compute throughput predictions for basic blocks. In addition, it also provides further insights into how basic blocks are executed, such as the port usage for each instruction.

To compare basic block throughput predictors, Chen et al. [12] proposed the BHive benchmark suite, along with a tool for measuring throughputs. We discovered that this benchmark suite contains a significant number of benchmarks with ambiguous throughputs that can give an unfair advantage to some of the tools. We therefore discard the corresponding benchmarks. Moreover, we discovered that the measurement tool often provides inaccurate measurements, and it is based on a different definition of throughput than most previous throughput predictors. We significantly improve the accuracy of the measurement tool, and we extend it to support both throughput definitions.

Using this improved benchmark suite and measurement methodology, we compare our throughput predictor with a number of previous tools on nine different Intel Core microarchitectures. In most cases, the average error of our tool is around or below 1%, which is significantly lower than the error of previous tools.

To summarize, the main contributions of our paper are:

- A parametric pipeline model that is applicable to all Intel Core microarchitectures released in the last ten years (Section 2).
- A throughput predictor (Section 3) that is more accurate than previous work by more than an order of magnitude on several recent microarchitectures (Section 5).

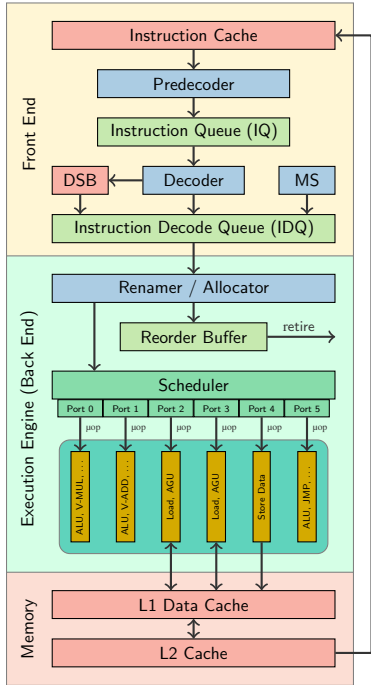


Figure 1: Pipeline of Intel Core CPUs

- An improved set of benchmarks for validating throughput predictors, and a more accurate measurement methodology (Section 4).

2. PIPELINE MODEL

Figure 1 shows the general structure of the pipelines of recent Intel Core CPUs. At such a high level, all these CPUs are very similar. For developing an accurate performance predictor, however, a more detailed model is necessary. Unfortunately, the official documentation only provides limited information on these details. Unofficial sources are not always correct, and also do not provide all of the necessary information at the required level of detail.

In this section, we describe the pipeline model that we have developed for accurate throughput prediction. Thus, the focus of the presentation is on those aspects that we have found to be relevant for predicting the performance of basic blocks. We describe the general structure and fill in the missing details. We obtained information on undocumented details through reverse engineering via microbenchmarks using hardware performance counters. For evaluating these microbenchmarks, we use nanoBench [13] and an extension to nanoBench that provides cycle-by-cycle performance data, similar to Brandon Falk’s “Sushi Roll” approach [14].

The model presented in this section is significantly more detailed than any previous models described in the literature. It is applicable to *all* Intel Core microarchitectures released in the last ten years; maybe surprisingly, the differences between these microarchitectures can be captured by a relatively small number of parameters.

2.1 Predecoding

The predecoder fetches aligned 16-byte blocks from the instruction cache (at most one such block per cycle), and it is

mainly responsible for detecting where each instruction begins. This is not completely straightforward, as an instruction can be between 1 and 15 bytes long, and detecting its length can require inspecting several bytes of the instruction.

The predecoded instructions are inserted into the *instruction queue* (IQ). The length of this queue is a parameter of our model; it is between 20 and 25 on recent microarchitectures.

According to our experiments, the predecoder can predecode at most five instructions per cycle on all of the microarchitectures we consider. If there are, e.g., six instructions in a 16-byte block, in the first cycle, five instructions would be predecoded, and in the next cycle, only one instruction would be predecoded. Several sources claim that the predecoding limit is six instructions per cycle [15, 16, 17]. This does not agree with our experiments. The source for the claims in [15, 16, 17] might be a section in Intel’s optimization manual [18] that mentions a limit of six instructions per cycle; however, this section is in a part of the manual that describes predecoding on old Intel Core 2 CPUs (which did not have a μ op cache, and thus decoding was a more significant bottleneck). The manual does not describe the predecoding limits for more recent microarchitectures.

A special case are instructions with a so called length-changing prefix (LCP). For such instructions, the predecoder has to use a slower length-decoding algorithm. This results in a penalty of three cycles for each such instruction.

For building an accurate simulator, it is important to know how instructions that cross a 16-byte boundary are predecoded; however, this is undocumented. Our experiments show that instructions are predecoded with the 16-byte block in which they end; they count toward the limit of five instructions in the corresponding cycle. We found that there is a one cycle penalty if five instructions were predecoded in the current cycle, the next instruction crosses a 16-byte boundary, but the primary opcode is contained in the current 16-byte block; if there are only prefixes or escape opcodes of the next instruction in the current block, there is no penalty.

Besides the difference in the length of the IQ, the predecoders appear to be identical on all CPUs that we consider.

2.2 Decoding

The decoding unit fetches up to four instructions from the IQ. It decodes the instructions into a sequence of μ ops and sends them to the *Instruction Decode Queue* (IDQ, sometimes also called *μ op queue*). The IDQ has between 28 and 70 entries on the microarchitectures we consider. This is a parameter of our model.

The decoding unit consists of one complex decoder and three simple decoders. The simple decoders can only decode instructions with one μ op. The complex decoder always decodes the first of the fetched instructions, and it can generate up to four μ ops. Instructions with more than four μ ops are (at least partially) handled by the Microcode Sequencer (see Section 2.5).

We discovered that there are instructions that have only one μ op but that can only be handled by the complex decoder, which was previously unknown. We have extended the benchmarking script from [19] so that it can detect all instructions that require the complex decoder automatically.

Several sources (e.g., [15, 16, 20]) claim that with the Sky-

lake microarchitecture, the number of simple decoders was increased from three to four. This does not agree with our experiments. However, with Skylake, the maximum number of μ ops that can be delivered from the decoding unit to the IDQ was increased from four to five (so, e.g., a 3- μ op and 2 1- μ op instructions can be decoded in the same cycle); the claims in [15, 16, 20] might be based on a misinterpretation of this change.

While the maximum number of μ ops that the decoding unit can deliver is documented, for implementing a simulator, it is also important to know in which cases this maximum can be achieved. According to previous work [16, 21], the number of instructions that can be decoded on simple decoders depends on the microarchitecture and on the number of μ ops of the instruction that is decoded by the complex decoder in the same cycle. We discovered that this number can also depend on the specific instruction that is decoded on the complex decoder, and not just its number of μ ops. We have extended the benchmarking script from [19] so that it can automatically determine for each instruction that requires the complex decoder the number of instructions that can be handled by simple decoders in the same cycle.

2.3 Macro-Fusion

The Instruction Queue (IQ) can merge specific pairs of instructions; such “macro-fused” instruction pairs are treated as single instructions in the rest of the pipeline. The first instruction of such a pair is always an arithmetic or logic instruction that updates the status flags, and the second instruction is a conditional jump instruction.

The actual pairs of instructions that can be macro-fused are microarchitecture-specific. Intel’s optimization manual [18] describes these pairs for Sandy Bridge and Haswell but not for more recent microarchitectures. We have therefore extended the script from [19] so that it can automatically find all instruction pairs that can be macro-fused.

We have found out that on pre-Skylake CPUs, instructions that are fusible cannot be sent to the last decoder; for Sandy Bridge and Ivy Bridge, this was also discovered by Agner Fog [21]. Whether fusible instructions can be sent to the last decoder is a parameter of our model.

2.4 Decoded Stream Buffer (DSB)

Decoded μ ops are stored in the *Decoded Stream Buffer* (DSB), also called the μ op cache. This can allow for a higher throughput of loops for which decoding is the bottleneck. The DSB can deliver between four and six μ ops per cycle to the IDQ; this is a parameter of our model.

A cache line in the DSB of a pre-Ice Lake CPUs can store at most six μ ops that need to be contained in the same 32-byte aligned code block. There can be at most three cache lines that contain μ ops from a specific 32-byte block. If a 32-byte block contains more than three cache lines, no μ op of this block will be stored in the DSB. There are a number of other restrictions; e.g., some μ ops require two slots in a cache line. These restrictions are not described in the official manuals, but they have been reverse engineered by Agner Fog [21].

We have discovered that on Skylake and Cascade Lake CPUs, μ ops from a specific 32-byte block are only served from the DSB if both 32-byte blocks of the corresponding

64-byte instruction cache line fulfill the restrictions described in the previous paragraph.

Starting with the Ice Lake microarchitecture, the DSB operates on 64-byte blocks. There can be at most six cache lines (with up to six μ ops each) from a specific 64-byte block. This was previously unknown.

As a workaround for the “Jump Conditional Code” (JCC) erratum, Skylake-based CPUs with a recent microcode cannot cache blocks that contain a jump instruction that crosses or ends on a 32-byte boundary [22].

According to [21], the “pipeline switches frequently between taking μ ops from the decoders and from the μ op cache”. We have found out that a switch from the decoders to the DSB can only take place after a branch instruction. Thus, for loops that contain only one branch instruction at the end, a switch to the DSB can only take place at the start of a loop iteration.

2.5 Microcode Sequencer (MS)

For instructions with more than four μ ops, up to four μ ops can be delivered from the decoding unit or the DSB, and the remaining μ ops will be delivered from the *microcode sequencer* (MS or MSROM) at a rate of four μ ops per cycle. While the microcode sequencer is active, no μ ops can be delivered from the decoders or the DSB.

It was previously unknown how many μ ops are delivered from the decoders (or the DSB) and how many from the MS for individual instructions. We have extended the script from [19] to automatically generate microbenchmarks for determining this distribution for individual instructions. We have discovered that there are also instructions with four or fewer μ ops that are delivered from the MS.

We discovered that when switching from the decoders to the MS and back, there are two stall cycles (in total). Switching from the DSB to the MS and back incurs two stall cycles on Skylake and its successors, and four stall cycles on earlier microarchitectures; this contradicts [21], which claims that “each switch may cost one clock cycle” on Sandy Bridge and Ivy Bridge. The number of stall cycles is a parameter of our model.

2.6 Loop Stream Detector (LSD)

The *Loop Stream Detector* (LSD) detects loops whose μ ops fit entirely into the IDQ. In this case, it locks the μ ops in the IDQ, and streams them continuously without requiring the DSB or the decoders.

The first μ op of the next loop iteration cannot be streamed in the same cycle as the last μ op of the current iteration. As this could be a significant bottleneck for small loops, the LSD can automatically unroll the loop. For the Ice Lake microarchitecture, Intel’s optimization manual [18] mentions this unrolling; it does however not describe how often the loop is unrolled for different loop sizes. For other microarchitectures, the manual does not provide information regarding this unrolling at all.

As the details of how this unrolling works are important for building a throughput predictor, we have developed microbenchmarks for analyzing how often the LSD unroll loops of different sizes. On Sandy Bridge and Ivy Bridge, the loops are not unrolled. For the more recent microarchitectures, we found three different variants. Which of these variants a

microarchitecture uses is a parameter to our model.

On Skylake-based CPUs, the LSD was disabled with a microcode update as a workaround for the SKL150 erratum [23].

2.7 Renamer / Allocator

The *renamer* (also called *Resource Allocation Table* (RAT)) maps architectural registers to physical registers. It also allocates resources for loads and stores, and it assigns execution ports to the μ ops (for more details on this, see Section 2.12).

The renamer fetches μ ops from the IDQ. It stores all μ ops in the reorder buffer (see Section 2.10), and it issues them to the scheduler (see Section 2.11). We call the maximum number of μ ops that the renamer can handle per cycle the *issue width*. The *issue width* is a parameter of our model, and it is either four (for most of the CPUs we consider), or five (for the two most recent microarchitectures).

The renamer can directly execute certain classes of μ ops like register moves (see Section 2.8), NOPs, or zero idioms; such μ ops are sent to the reorder buffer but not to the scheduler. Zero idioms are instructions that always set the target register to 0, independently of the value in the input registers. An example is an XOR of a register with itself.

2.8 Move Elimination

Starting with the Ivy Bridge microarchitecture, certain register-to-register move instructions can be executed by the renamer (see Section 2.7).

However, on pre-Ice Lake CPUs, this *move elimination* is not always successful. It was previously not known in which cases move elimination is not possible. [21] and [16] claim that it fails when the operands are not ready. This is incorrect. Intel’s manual [18] mentions “internal resource constraints” that may prevent move eliminations, and provides an example in which only 50% of the moves could be eliminated, but it does not describe these internal resources in more detail.

The relevant Intel CPUs have performance counters that count the number of eliminated and non-eliminated move instructions. We have developed microbenchmarks that use these performance counters to analyze when move elimination is successful. The following model agrees with our observations. The processor keeps track of the physical registers that are used by more than one architectural register. We say that each such physical register occupies one *elimination slot*. On the relevant CPUs, there are four such slots for general-purpose registers, and four slots for vector registers. An elimination slot is released again after the corresponding registers have been overwritten. The number of move instructions that can be eliminated in a cycle depends both on the number of available elimination slots, and on the number of successful eliminations in the previous cycle.

We have discovered that on Tiger Lake and Ice Lake CPUs with a recent microcode, move elimination for general-purpose registers is disabled. On Ice Lake CPUs with an older microcode, move elimination is enabled. We suppose that it has been disabled due to the ICL065 erratum [24], which states that “under complex micro-architectural conditions, when Move Elimination is performed, unpredictable system behavior may occur.”

2.9 Micro-Fusion

Micro-fusion is an optimization in which two μ ops are fused together and treated as one μ op in the early parts of the pipeline; they are split into two μ ops before execution in the back end. All decoders (including the simple decoders) can emit micro-fused μ ops. Only specific types of μ ops can be fused; one of the μ ops must be a load or store μ op. We have extended the benchmarking script from [19] to automatically determine the number of fused μ ops for each instruction.

There are two possible locations in the pipeline where micro-fused μ ops may be split into their components. In most cases, micro-fused μ ops are split when they enter the scheduler; however, they take only one slot in the reorder buffer.

In some cases, micro-fused μ ops from instructions that use an indexed addressing mode are split already by the renamer; Intel’s optimization manual refers to this as “unlamination”. Unlaminated μ ops require two slots in the reorder buffer. If the number of μ ops after unlamination exceeds the issue width, the renamer issues both μ ops that were part of the fused μ op in the next cycle. This was previously unknown. The details regarding in which cases μ ops are unlaminated are microarchitecture specific, and not documented in Intel’s manual for post-Haswell microarchitectures. We have extended the script from [19] to automatically detect the instruction variants for which unlamination occurs.

2.10 Reorder Buffer

All μ ops remain in the reorder buffer until they are ready to retire. A μ op is ready to retire if it has finished execution and all older μ ops (in program order) are ready to retire.

The reorder buffers of the microarchitectures we consider have between 168 and 352 entries; this is usually documented.

The number of μ ops that can be retired per cycle is usually not documented. Therefore, we have developed microbenchmarks for measuring it. On the CPUs we consider, it is between four and eight.

Both the size of the reorder buffer and the number of μ ops that can be retired per cycle are parameters of our model.

2.11 Scheduler

The scheduler (also called the reservation station) keeps track of the dependencies of the μ ops. Once all operands of a μ op are ready, the scheduler dispatches it to its assigned port (see Section 2.12).

Each port is connected to a set of different functional units, such as an ALU, an address-generation unit (AGU), or a unit for vector multiplications. Each port can accept at most one μ op in every cycle. However, as most functional units are fully pipelined, a port can typically accept a new μ op in every cycle, even though the corresponding functional unit might not have finished executing a previous μ op.

The microarchitectures we consider have between six and ten ports; this is a parameter of our model. The schedulers of the microarchitectures we consider have between 54 and 160 entries, which is also a parameter of our model.

We discovered that a μ op cannot be dispatched to a port earlier than five cycles after it has been issued by the renamer.

2.12 Port Assignment

Previous work [19, 25, 26] has identified the ports that the μ ops of individual instructions can use. For μ ops that can use more than one port, it was, however, previously unknown how the actual port is chosen by the processor. We reverse engineered the port assignment algorithm using microbenchmarks. In the following, we describe our findings for CPUs with eight ports; such CPUs are currently most widely used.

The ports are assigned when the μ ops are issued by the renamer to the scheduler. In a single cycle, up to four μ ops can be issued. In the following, we will call the position of a μ op within a cycle an *issue slot*; e.g., the oldest instruction issued in a cycle would occupy issue slot 0.

The port that a μ op is assigned depends on its issue slot and on the ports assigned to μ ops that have not been executed and were issued in a previous cycle.

In the following, we will only consider μ ops that can use more than one port. For a given μ op m , let P_{min} be the port to which the fewest non-executed μ ops have been assigned to from among the ports that m can use. Let $P_{min'}$ be the port with the second smallest usage so far. If there is a tie among the ports with the smallest (or second smallest, respectively) usage, let P_{min} (or $P_{min'}$) be the port with the highest port number from among these ports (the reason for this choice is probably that ports with higher numbers are connected to fewer functional units). If the difference between P_{min} and $P_{min'}$ is greater or equal to 3, we set $P_{min'}$ to P_{min} .

The μ ops in issue slots 0 and 2 are assigned to port P_{min} . The μ ops in issue slots 1 and 3 are assigned to port $P_{min'}$.

A special case are μ ops that can use port 2 and port 3. These ports are used by μ ops that handle memory accesses, and both ports are connected to the same types of functional units. For such μ ops, the port assignment algorithm alternates between port 2 and port 3.

3. THROUGHPUT PREDICTOR

Based on the model from Section 2 and the instruction data from [19], we have implemented a tool, called uiCA (“uops.info Code Analyzer”), that simulates the execution of basic blocks on Intel Core microarchitectures. In addition to providing throughput predictions, uiCA can also generate a table that contains the port usage for each instruction, and it can output a timeline that shows what happens in each cycle.

Throughput predictions for a basic block are obtained as follows. The tool simulates the repeated execution of the basic block for at least 500 cycles and until at least 10 iterations have been completed. Let n be the number of completed iterations. Let t be the cycle in which the last instruction of the n -th iteration was retired, and t' be the cycle in which the last instruction of the $\frac{n}{2}$ -th iteration was retired. The tool then predicts $\frac{2 \cdot (t - t')}{n}$ as the throughput. This approach is similar to the approach proposed in [13]. It is based on the assumption that after $\frac{n}{2}$ iterations, a steady state has been reached.

4. BENCHMARKS AND MEASUREMENTS

To evaluate and compare our simulator to previous approaches, we need a set of suitable benchmarks. Chen et al. [12] proposed the BHive benchmark suite, which is designed specifically to evaluate basic block throughput predic-

tors on x86 systems. The BHive suite contains more than 300,000 basic blocks that were extracted from applications from different domains, including numerical computation, databases, compilers, machine learning, and cryptography.

In addition to that, Chen et al. in the same paper also propose a profiling tool to measure the throughput of such basic blocks using hardware performance counters. In contrast to previous tools, their tool can automatically profile basic blocks that may perform arbitrary memory accesses. This is implemented by mapping all accessed virtual pages to a single physical page, which also ensures that most memory accesses (after a warm-up run) result in hits in the L1 cache. In addition to measuring the execution time, the tool also monitors several other performance counters; this is used to detect measurements with instruction or data cache misses, unaligned loads, or context switches. The measurements are repeated multiple times. If there are too many measurements with caches misses, unaligned loads, or context switches, or if the measurement results are not stable enough, the corresponding basic block is removed from the benchmark suite. Otherwise, the minimum of the measured times is reported as the throughput. Chen et al.’s tool was also used to measure the throughputs of the basic blocks that were used to train Ithemal [10] and DiffTune [11].

While Chen et al.’s benchmark suite and measurement framework appear to be suitable for evaluating the work presented in our paper, we discovered a number of issues with their approach that can lead to incorrect or misleading results. In particular, the notion of throughput their measurement tool is based on is different from the notion of throughput that previous tools like IACA use. Moreover, Chen et al. seem to assume that there is one *true* throughput for all of the benchmarks they consider. This is incorrect. In general, the throughput of a basic block can depend both on the initial architectural and microarchitectural state. In this section, we look at these issues in detail. In particular, we describe how important parameters of the initial state can be controlled. Wherever possible, we propose canonical values for these parameters that do not contradict modeling assumptions of previous tools. We remove benchmarks for which this is not possible. Furthermore, we identify several classes of benchmarks which are not meaningful for comparing different predictors. In addition to that, we propose an improved measurement infrastructure.

4.1 Definitions of Throughput

Intel’s IACA considers the throughput of a basic block to be the average number of clock cycles per iteration when executing the basic block repeatedly in a loop at a steady state, assuming that all memory accesses are cache hits. Thus, it is intended to be used to analyze basic blocks that end with a branch instruction that jumps back to the beginning of the loop; all examples in IACA’s user guide [1] are of this form (IACA does not reject basic blocks that are not of this form; however, the behavior in such a case is not specified in the documentation).

Chen et al. claim to use “IACA’s definition of throughput” [12]. However, their measurement framework only considers basic blocks that do not end with a branch instruction. They consider the throughput to be the average number of cy-

cles (per execution of the basic block) when unrolling the basic block a sufficient number of times to reach a steady state.

An important difference between these two definitions is that in the first case, the μ ops of many benchmarks are delivered by the DSB or the LSD (see Section 2), whereas in Chen et al.’s measurement tool, all μ ops have to go through the decoders, which can be significantly slower. As an example, consider the basic block

```
ADD AX, 0x1234; DEC R15
```

When unrolling this code sequence multiple times, the average execution time on a Skylake CPU is 3.44 cycles per iteration; the bottleneck here is a stall in the predecoder (see Section 2.1). On the other hand, the code sequence

```
loop: ADD AX, 0x1234; DEC R15; JNZ loop
```

is served from the DSB and requires, on average, only 1 cycle per loop iteration, even though it has an additional instruction.

OSACA [6, 7] and CQA [9] are based on the same definition as IACA; CQA can only analyze code that ends with a branch instruction.

For llvm-mca, it is not completely clear which definition is used. According to the documentation, llvm-mca “simulates the execution of the machine code sequence in a loop of iterations” [8]; however, the examples in the documentation do not end with a branch instruction. As llvm-mca does not model performance bottlenecks in the front end, the throughput predictions can generally be expected to be closer to IACA’s definition.

4.1.1 Our Definition

Our tool predicts the throughput of basic blocks that end with a branch instruction according to the first definition. For basic blocks that do not end with a branch instruction, it predicts the throughput according to Chen et al.’s definition.

4.2 Extending BHive

Using their profiling tool, Chen et al. measured the throughput of the benchmarks in the BHive suite (which do not end with a branch instruction). They then compare the predictions of IACA, OSACA, and llvm-mca with the predictions of Ithemal, which was trained on benchmarks that were evaluated with the same profiling tool (i.e., using unrolling). As the predictions of Ithemal are closer to the measurements than the predictions of the other tools, they conclude that Ithemal “outperforms” the other tools.

We don’t think this conclusion is valid because the measurements are based on a different definition of throughput than the predictions of the other tools.

In order to enable a more meaningful comparison with previous tools, we have created a variant of the BHive benchmark suite in which the benchmarks end with a branch instruction. In the following, we will call this benchmark suite $BHive_L$, and the original benchmark suite $BHive_U$.

We have generated the benchmarks in $BHive_L$ from those in $BHive_U$ as follows. Let B be a benchmark in $BHive_U$, and let R_x be a general-purpose register that is not used by B . We then add to $BHive_L$ an extended benchmark of the form

```
loop: B; DEC Rx; JNZ loop
```

Here, R_x is used as the loop counter. For a small number of benchmarks in $BHive_U$, we could not find such a register R_x , as these benchmarks already use all general-purpose registers. We omitted these benchmarks from $BHive_L$.

Several of the benchmarks in $BHive_U$ are very small; some of them consist of only a single instruction. For such benchmarks, the execution time of the extended benchmark may be dominated by the loop overhead, which limits the throughput to 1 iteration per cycle in the best case. Therefore, for benchmarks B with fewer than five instructions, we added an additional variant in which B is unrolled until there are at least five instructions (which corresponds to the maximum issue width of the CPUs that we consider) in the body of the loop.

We have extended Chen et al.’ profiling tool to support evaluating the benchmarks in $BHive_L$.

4.3 Problematic Benchmarks

4.3.1 Benchmarks with Input-Dependent Throughput

For several benchmarks, the throughput depends on the initial values of the registers and memory locations.

This is, e.g., the case for benchmarks that use instructions with input-dependent latency or throughput, such as instructions that use the divider unit, or the CPUID instruction. For an integer division, for example, there can be a difference of more than 60 cycles depending on the input values. The CPUID instruction requires between around 100 cycles and almost 2,000 cycles, depending on the input.

For benchmarks containing division instructions, IACA typically predicts a throughput that corresponds to input values that lead to a slow division. On the other hand, the values that Chen et al.’s measurement tool uses to initialize registers and memory locations tend to lead to fast divisions. In [10, 12], the measured values were considered to be the *correct* values, and IACA’s values were considered to be *incorrect*. This does not allow for a fair comparison between different tools. We therefore removed benchmarks that use the divider units, and benchmarks that contain the CPUID instruction from the benchmark suite.

Another, maybe somewhat less obvious class of benchmarks with input-dependent throughput are benchmarks that both read from and write to potentially the same memory address. Consider for example the following benchmark:

```
MOV [R9], R8; MOV R8, [R10]
```

If registers R9 and R10 contain the same address, there is a read-after-write dependency on the corresponding memory location, and the throughput is about 5 cycles per iteration on a Haswell machine. If R9 and R10 contain addresses that are different (and do not differ by a multiple of 4096), there is no such dependency, and the throughput is 1 cycle per iteration. If the addresses are separated by a multiple of 4096, there can be a penalty due to so called “4K aliasing” [18].

IACA, OSACA, llvm-mca, and CQA predict a throughput of around 1 cycle per iteration for this benchmark. Chen et al.’s measurement tool measures a throughput of around 5 cycles per iteration. This is because this tool initializes all general-purpose registers with the same value, and hence, there is a read-after-write dependency.

Thus, such benchmarks are not useful for comparing previous tools with measurements, and therefore, we removed all

benchmarks that read from and write to memory, and that use either different address registers for the read and the write, or that use a register that is modified by the benchmark. We did not remove benchmarks that use the same address registers for reading and writing to memory and that do not modify this register, as these benchmarks always have a read-after-write dependency, independently of the initial values in the address registers.

On Ice Lake and Tiger Lake CPUs, two stores can be executed in the same cycle, but only if they are to the same cache line [18]. For these two microarchitectures, we therefore also removed benchmarks, for which it may depend on initial values whether two stores are to the same cache line.

On Sandy Bridge and Ivy Bridge CPUs, two load operations can only be executed in the same cycle if they do not have a bank conflict [18, 27]. A bank conflict occurs if two load operations access different cache sets, but the bits 2–5 of their addresses are identical. Thus, whether a bank conflict occurs can also depend on the initial value in the address registers. Sandy Bridge and Ivy Bridge CPUs have a performance counter for bank conflicts. We extended Chen et al.’s measurement tool such that it can access these counters, and we reject benchmarks with bank conflicts on these two microarchitectures.

4.3.2 TLB Misses

As described before, Chen et al.’s measurement tool maps all accessed virtual pages to the same physical page to prevent cache misses. While this approach indeed prevents cache misses, it does, however, not prevent TLB misses if a benchmark accesses a large number of virtual pages. This issue was acknowledged by the authors. We extended the measurement tool such that it also monitors TLB-related performance counters, and we reject benchmarks that lead to TLB misses.

4.3.3 Unbalanced x87 Operations

The x87 floating-point registers are organized as a stack. The BHive suite contains several basic blocks that contain an unbalanced number of push or pop operations to this stack. Correct programs would not execute such benchmarks repeatedly in isolation, as this leads to stack underflows or overflows, which result in penalties of hundreds of cycles. It is worth noting that the basic blocks in the BHive benchmark suite are not necessarily executed in loops in the applications from which they were extracted.

While predicting the penalties due to underflows or overflows would not be difficult, we think that using such benchmarks for a comparison with previous tools would provide an unfair advantage, as previous tools are typically intended to analyze correct programs. We therefore removed such benchmarks from the BHive suite.

Another important consideration regarding x87 instructions is the initial state of the stack. A canonical choice for this is to start with an empty stack. There are several benchmarks that have a balanced number of push and pop operations, but that perform a pop operation before the first push operation. We also removed such benchmarks from the benchmark suite, as they would lead to an underflow in the first iteration.

4.3.4 Unsupported Instructions

The TZCNT instruction was introduced with the Haswell microarchitecture. It has the same encoding as the BSF instruction with a REP prefix. This prefix is undefined for the BSF instruction; however, older CPUs do not generate an exception in this case, but simply ignore the prefix.

We removed the TZCNT instruction from the benchmarks for older microarchitectures, as it is not meaningful to evaluate throughput predictions on unsupported instructions.

4.4 Initial Microarchitectural State

4.4.1 Initial State of Buffers and First Issue Slot

The throughput of a benchmark can be affected by the initial state of the buffers in the front end, and by the issue slot that is used by the first μ op of the benchmark. Consider for example the following benchmark:

```
NOP; CMP RAX, RAX; NOP; XOR RAX, RBX
```

The XOR and CMP instructions have a read-after-write dependency on the XOR from the previous iteration. However, the XOR instruction does not have a dependency on the CMP instruction. On, e.g., a Skylake machine (which can issue 4 μ ops per cycle), the XOR and CMP instructions (which both can use ports 0, 1, 5, and 6) of one iteration are always assigned the same ports (see Section 2.12) if the first issue slot is 0. Hence, when register RAX becomes ready, the following XOR and CMP instructions compete for the same port. On the other hand, if the first issue slot is 1, the XOR and CMP instructions of one iteration are typically assigned different ports, and thus, do not compete. Note that this effect does not just affect the first iterations of the benchmark, but can last indefinitely.

A canonical choice for the first issue slot that does not contradict modeling assumptions in previous tools is 0.

For the initial state of the front-end buffers, there are two possible canonical choices: one can start with full buffers or empty buffers. We are not aware of an obvious way to completely fill the buffers. Therefore, we chose to start with empty buffers. This can be achieved by executing a long enough sequence of 15-byte NOP instructions before executing the benchmark. These instructions will create a bottleneck in the predecoder, which will drain the front end buffers. Furthermore, this also ensures that the issue slot for the first instruction of the benchmark is 0.

Another advantage of starting with empty buffers is that this way, often a steady state will be reached faster. If we start with full buffers, then a benchmark with a bottleneck in the front end will slowly drain the buffers; when they become empty, the performance characteristics of the benchmark change. On the other hand, if we start with empty buffers and consider a benchmark with a bottleneck in the back end, then the buffers will slowly fill up; however, the performance characteristics of the benchmark do not change when the buffers are completely full.

4.4.2 Initial State of Move Elimination Resources

The number of move elimination slots (see Section 2.8) that are in use at the beginning of executing a benchmark can also have a significant influence on the execution time. If, for example, all the elimination slots are in use, and the

benchmark does not overwrite any of the registers that occupy the renaming slots, then no move instruction in the benchmark can be eliminated.

A canonical choice for the initial state of the elimination slots is to assume that all of them are available. This is straightforward to achieve by just overwriting all registers before executing the benchmark.

4.4.3 Alignment

As the predecoder and the DSB work with aligned 16-byte, 32-byte, and 64-byte blocks, the alignment offset of the first instruction of a benchmark relative to such a block can have a significant influence on the throughput. Chen et al. did not consider this issue. The alignment offset that their tool uses is unspecified and may change if unrelated parts of their tool are modified.

In our tool, the alignment offset (relative to 64-byte cache line) can be specified via a parameter. For the measurements, we modified Chen et al.’s tool such that it uses an alignment offset of 0. This choice does not contradict modeling assumptions in previous prediction tools.

4.5 Performing Accurate Measurements

For a meaningful comparison of measurements to predictions, it is important that the measurements are performed in an accurate way.

Based on our experience, measurements using hardware performance counters can be almost cycle-accurate if a number of precautions are taken. Unfortunately, Chen et al.’s tool does not achieve this accuracy. Skylake CPUs, for example, can execute at most two instructions with memory operands per cycle. Thus, any measurement with a throughput value smaller than 0.5 cycles per iteration for benchmarks with memory instructions is obviously not accurate. Chen et al.’s published measurements file, which was used for the evaluation in [12], contains almost 20,000 such cases. More than 2,200 of them even report a throughput value of less than 0.45 cycles per iteration (i.e., the measurements are more than 10% off from the correct value). There are multiple reasons for these inaccuracies that we will discuss in the following.

Chen et al.’s tool executes multiple branch instructions on the critical path (i.e., while performance counting is active). This makes the execution time dependent on the state of the branch predictor, which, in general, leads to unpredictable measurements. We removed all branches from the critical path using a similar approach as described in [13].

The RDPMC instruction that reads the performance counters is not a serializing instruction on recent Intel CPUs; thus, it can be reordered with earlier or later instructions. For meaningful measurements, it is important to insert a serializing instruction before and after each execution of the RDPMC instruction. In Chen et al.’s implementation, one of the required serializing instructions is missing; we added the corresponding instruction. In the other cases, Chen et al. use the CPUID instruction for serialization. As discussed in Section 4.3.1, this instruction is relatively expensive and has an input-dependent throughput. Recent work [13, 28] recommends to use the LFENCE instruction instead; we changed the implementation accordingly.

For small basic blocks, Chen et al. determine the through-

put as the difference between the measured execution times for 100 and 200 repetitions of the basic block, divided by 100. These measurements can be too short to obtain meaningful results. Consider, for example, a benchmark with only one instruction. Depending on the instruction, the execution time for 100 repetitions might be as low as 25 cycles. A measurement error of just one cycle already leads to a difference of 4% for such a benchmark. Also, such a small number of repetitions might not be sufficient to reach a steady state; as discussed in Section 2, the reorder buffer, for example, can have up to 352 entries on recent microarchitectures.

For *BHive_U*, we use the following approach instead. Let n be the number of instructions in a benchmark, and let $r := \lceil \frac{500}{n} \rceil$. Then we determine the throughput as the difference between the measured execution times for r and $2 \cdot r$ many repetitions, divided by r . This leads to a significantly higher repetition count than Chen et al.’s approach for most benchmarks, but it is still small enough so that the code fits in the instruction cache (the instruction caches on the CPUs we consider have a size of at least 32 kB, and x86 instructions can be at most 15 bytes long).

For *BHive_L*, we use the difference between 10,000 and 20,000 iterations, divided by 10,000.

We repeat all throughput measurements 100 times. We then remove the top and bottom 20% of the measured values, which might be outliers due to, e.g., interrupts. If the minimum and the maximum of the remaining throughput values differs by more than 0.02 cycles, we reject the benchmark, as the measurements were not stable. Otherwise, we use the median of the measurements as the throughput.

We perform all measurements with all but one core disabled to prevent disturbances from other processes.

With our improvements, there are no more benchmarks with memory operands that have a measured throughput that is smaller than 0.5 cycles per iteration.

4.6 Size of Improved Benchmark Set

After excluding the benchmarks described in the previous sections, *BHive_U* contains between 135,915 (for Ivy Bridge) and 193,777 (for Tiger Lake) benchmarks, and *BHive_L* contains between 330,503 (for Rocket Lake) and 352,118 (for Cascade Lake) benchmarks. This is still a very large number of benchmarks, which allows for a meaningful comparison of different throughput prediction tools.

5. EVALUATION

5.1 Comparison with Other Tools

In this section we compare our tool, *uiCA*, with several previous tools on all major Intel Core microarchitecture generations that were released in the last ten years, from Sandy Bridge (released in 2011) to Tiger Lake (released in 2020).

We use IACA [1] in versions 2.3 and 3.0; version 3.0 does not support the older microarchitectures, and we noticed that IACA 2.3 tends to provide more accurate predictions. For *llvm-mca*, we use version 10.0.0; for the microarchitectures that are supported by DiffTune, we additionally also evaluate *llvm-mca* in version 8.0.1, as DiffTune is based on this version. We use DiffTune [11] at commit 9992f69 with the mod-

els from the paper, which are provided at¹. We use Ithelmal at commit 47a5734 with the retrained models from the BHive paper². For CQA, we use version 2.13.2. We use OSACA at commit 63563ec; we do not use the latest released version of OSACA, as we found several bugs in this version that we reported and that were since fixed by the authors. In cases in which a tool crashes or does not return a result within a timeout of one hour, we consider the throughput prediction to be 0.

To compare the different tools, we use the same metrics that were used in [11, 12]:

- The mean absolute percentage error (MAPE) of the predictions relative to the measurements.
- Kendall’s Tau coefficient [29], which is a measure for how well the pairwise ordering is preserved. As argued by Chen et al. [12], Kendall’s Tau coefficient can be more useful than the MAPE for example for compiler optimizations, where the relative ordering of different candidate programs is more important than their absolute execution times.

As a baseline, we consider the following. Let n be the number of instructions in a specific benchmark, and let m_r and m_w be the number of memory read and write accesses of this benchmark. Furthermore, let i be the issue width (see Section 2.7) of the corresponding microarchitecture, and let w be the number of memory write operations that can be performed per cycle.

For $BHive_U$, we use

$$\max\left(\frac{n}{4}, \frac{m_r}{2}, \frac{m_w}{w}\right)$$

as the baseline for the throughput prediction of this benchmark. This value constitutes a lower bound on the execution time of basic blocks without branch instructions, as at most four instructions can be decoded per cycle, and at most two memory read operations can be performed per cycle on all microarchitectures we consider.

For $BHive_L$, we use

$$\max\left(1, \frac{n-1}{i}, \frac{m_r}{2}, \frac{m_w}{w}\right)$$

as the baseline. We use $n-1$ instead of n , as the decrement and branch instructions at the end of each benchmark in $BHive_L$ are usually macro-fused; we use 1 as an additional lower bound, as the benchmarks in $BHive_L$ cannot run faster than one iteration per cycle due to the read-after-write dependency of the decrement operation.

Table 1 shows the results of our evaluation. For completeness and consistency with the evaluations in [11, 12], we also evaluated the tools that are intended to analyze loops on $BHive_U$ (except for CQA, which can only analyze code that ends with a branch instruction).

In most cases, the accuracy on $BHive_L$ is higher than on $BHive_U$; the exception here are Ithelmal and DiffTune, which were trained on measurements that were obtained by unrolling. This shows that, for a meaningful comparison, it is important that measurements and predictions are based on the same definition of throughput (as discussed in Section 4.1).

Our tool, uiCA, provides the most accurate predictions in

all cases. In many cases, the MAPE is lower by an order of magnitude or more compared to the best previous tools. For uiCA, Kendall’s Tau coefficient is always higher than for the previous tools; in most cases, it is significantly higher.

On the Cascade Lake, Skylake, Broadwell, and Haswell microarchitectures, the accuracy of OSACA was similar to several other previous tools. On Ice Lake, Ivy Bridge, and Sandy Bridge, however, the accuracy is significantly below the baseline. A possible explanation for this is that for these microarchitectures, there is a relatively large number of instructions that are currently not supported by OSACA; in such cases, OSACA simply ignores these instructions.

Ithelmal cannot analyze code that ends with a branch instruction; for the evaluation of Ithelmal on $BHive_L$, we therefore removed the branch instruction, but we kept the instruction that decrements the loop counter in each iteration. On $BHive_U$, Ithelmal provides the best predictions among the previous tools; however, the predictions of uiCA are significantly better. On $BHive_L$, several other previous tools provide better predictions than Ithelmal; in two cases the MAPE is even below the baseline. It is likely that retraining Ithelmal on measurements obtained with the methodology described in Section 4 would improve its accuracy on $BHive_L$. However, we were unable to do so, as the training set is not publicly available.

Unlike in the evaluation in [11], DiffTune does not perform better than llvm-mca on the set of benchmarks we consider. Moreover, DiffTune’s accuracy is on all supported microarchitectures below the baseline; on the Skylake and Haswell microarchitectures, the MAPE for $BHive_L$ is more than an order of magnitude higher than that of the baseline.

5.2 Influence of Different Components

We now evaluate how important different components of the model proposed in Section 2 are for obtaining accurate throughput predictions. In Table 2, we compare different variants of our tool in which parts of the model were replaced by simpler implementations. We use the Cascade Lake microarchitecture, which is the most recent microarchitecture for which move elimination has not been disabled (Section 2.8).

In the first variant, we replace our front-end model with one that is unbounded and can always deliver the maximum number of μ ops to the renamer. This is similar to the front-end models used by many previous tools. For $BHive_U$, this leads to a huge increase in the average error. For $BHive_L$, the increase is smaller, which is as expected, since for these benchmarks, the μ ops are often delivered from the LSD or the DSB, which has a higher bandwidth than the decoders; however, the error is still almost an order of magnitude higher than with our detailed front-end model from Section 2.

For the second variant, we replace the port assignment algorithm described in Section 2.12 with one that randomly selects (with uniform probability) a port from among the ports that a μ op can use. This is similar to the approach described in [6]. For $BHive_U$, this leads to an error that is almost five times as high, and for $BHive_L$, to an error that is more than 17 times as high. A main reason for the higher error in the second case is probably that taken branch instructions can only use port 6; with the random port algorithm there is more competition for port 6 from μ ops which can also use other

¹<https://github.com/ithelmal/DiffTune/issues/1>

²<https://github.com/ithelmal/Ithelmal-models/tree/master/bhive>

Table 1: Comparison of different tools on $BHive_U$ and $BHive_L$

Microarchitecture (CPU)	Predictor	$BHive_U$		$BHive_L$	
		MAPE	Kendall's Tau	MAPE	Kendall's Tau
Rocket Lake (Core i9-11900)	uiCA	0.54%	0.9841	0.96%	0.9750
	Baseline	15.50%	0.7397	9.26%	0.7808
Tiger Lake (Core i7-1165G7)	uiCA	1.06%	0.9744	1.01%	0.9727
	llvm-mca-10	25.74%	0.7049	13.80%	0.8486
	Baseline	17.49%	0.7245	11.25%	0.7413
Ice Lake (Core i5-1035G1)	uiCA	1.08%	0.9744	0.80%	0.9754
	OSACA	53.80%	0.3143	21.98%	0.4698
	llvm-mca-10	25.38%	0.7030	13.64%	0.8512
	CQA			6.74%	0.8835
	Baseline	17.54%	0.7230	10.84%	0.7510
Cascade Lake (Core i9-10980XE)	uiCA	0.49%	0.9699	0.69%	0.9819
	llvm-mca-10	23.17%	0.7211	13.21%	0.8060
	OSACA	20.83%	0.7511	11.61%	0.8068
	Baseline	15.49%	0.7461	10.31%	0.8021
Skylake (Core i7-6500U)	uiCA	0.48%	0.9789	0.38%	0.9894
	Ithemal	8.28%	0.8172	13.66%	0.7582
	IACA 3.0	13.49%	0.7802	14.26%	0.8290
	IACA 2.3	11.85%	0.8071	8.42%	0.8477
	OSACA	14.95%	0.7639	11.25%	0.8045
	llvm-mca-10	15.61%	0.7258	12.01%	0.8015
	llvm-mca-8	15.39%	0.7434	11.98%	0.8021
	DiffTune	24.48%	0.6626	104.88%	0.6426
	CQA			7.44%	0.8847
	Baseline	17.28%	0.7228	10.03%	0.7999
Broadwell (Core i5-5200U)	uiCA	1.08%	0.9805	0.62%	0.9839
	IACA 3.0	14.69%	0.8012	11.47%	0.8725
	IACA 2.3	13.22%	0.8206	5.84%	0.8928
	OSACA	17.52%	0.7456	9.69%	0.8365
	llvm-mca-10	14.23%	0.7793	16.71%	0.8286
	CQA			5.03%	0.9213
	Baseline	16.97%	0.7572	7.44%	0.8332
Haswell (Xeon E3-1225 v3)	uiCA	0.77%	0.9850	0.60%	0.9840
	Ithemal	7.38%	0.8400	16.19%	0.7700
	IACA 3.0	15.04%	0.8080	12.00%	0.8733
	IACA 2.3	13.13%	0.8291	5.79%	0.8925
	OSACA	17.84%	0.7463	9.77%	0.8307
	llvm-mca-10	20.29%	0.7835	18.97%	0.8259
	llvm-mca-8	21.08%	0.7784	19.46%	0.8171
	DiffTune	24.80%	0.6997	138.47%	0.6925
	CQA			5.08%	0.9220
	Baseline	17.30%	0.7604	7.57%	0.8314
Ivy Bridge (Core i5-3470)	uiCA	1.52%	0.9607	1.12%	0.9494
	Ithemal	7.08%	0.8212	12.43%	0.7785
	IACA 2.3	13.94%	0.7739	11.54%	0.8271
	OSACA	36.23%	0.4884	24.88%	0.5846
	llvm-mca-10	22.79%	0.7656	20.76%	0.8154
	llvm-mca-8	22.93%	0.7622	20.76%	0.8138
	DiffTune	26.21%	0.6470	82.94%	0.7516
	CQA			4.05%	0.9174
Baseline	18.81%	0.7243	14.47%	0.7670	
Sandy Bridge (Core i7-2600)	uiCA	1.91%	0.9612	0.99%	0.9648
	IACA 2.3	11.91%	0.8194	9.95%	0.8482
	OSACA	36.85%	0.5311	24.75%	0.5659
	llvm-mca-10	22.67%	0.8069	18.34%	0.8455
	CQA			4.08%	0.9238
	Baseline	20.28%	0.7517	15.56%	0.7577

Table 2: Influence of the simulation of different microarchitectural components on the prediction accuracy

Microarchitecture	Predictor	<i>BHive_U</i>		<i>BHive_L</i>	
		MAPE	Kendall’s Tau	MAPE	Kendall’s Tau
Cascade Lake (all benchmarks)	uiCA	0.49%	0.9699	0.69%	0.9819
	uiCA with simple front end	8.57%	0.8602	6.23%	0.9048
	uiCA with simple port assignment	2.38%	0.9279	12.23%	0.8608
	uiCA without micro-fusion	8.80%	0.8673	3.32%	0.9544
	uiCA without macro-fusion	0.49%	0.9699	8.93%	0.8851
	uiCA without LSD unrolling	0.49%	0.9699	6.72%	0.9245
Cascade Lake (benchmarks with moves)	uiCA	0.47%	0.9796	0.51%	0.9827
	uiCA without move elimination	1.70%	0.9663	1.73%	0.9608
	uiCA with full move elimination	0.54%	0.9795	0.54%	0.9837

ports, and which would more frequently be scheduled on one of these other ports by the algorithm from Section 2.12.

For the third variant, we assume that μ ops from the same instruction cannot be micro-fused by the decoders. For *BHive_L*, this leads to an error that is about five times as high. For *BHive_U*, the error is almost 18 times as high; the main reason for this is likely that all instructions that are normally decoded to one micro-fused μ op now require the complex decoder.

In the fourth variant, we assume that instructions cannot be macro-fused. For *BHive_U*, this makes no difference, as these benchmarks contain no branch instructions. For *BHive_L*, on the other hand, the error increases by more than an order of magnitude.

In the next variant, the LSD does not perform the unrolling described in Section 2.6. Again, this leads to no difference for *BHive_U*, as these benchmarks do not use the LSD. For *BHive_L*, the error is almost an order of magnitude higher.

Finally, we evaluate the influence of the move elimination approach described in Section 2.8. For this, we consider only benchmarks that actually contain move instructions, which is the case for more than one third of the benchmarks. We consider two variants. In the first variant, no move instructions are eliminated. This leads to an average error that is more than three times as high. In the second variant, all eligible move instructions are eliminated. For *BHive_U*, this leads to an error that is about 15% higher, and for *BHive_L* to an error that is about 6% higher.

6. RELATED WORK

6.1 Throughput Predictors

The Intel Architecture Code Analyzer (IACA) [1] is a tool developed by Intel that can statically analyze the performance of loop kernels on several older microarchitectures. The tool generates a report which includes throughput and port usage data of the analyzed loop kernel. As the tool is closed source, its underlying model and prediction methodology is unknown. In April 2019, Intel announced IACA’s end of life.

The Open Source Architecture Code Analyzer (OSACA) [6, 7] is an analytical performance prediction tool for Intel, AMD, and ARM microarchitectures. It is based on a relatively coarse-grained model of these microarchitectures; according to [7], “accurately modeling the performance characteristics

of the decode, reorder buffer, register allocation/renaming, retirement and other stages, which all may limit the execution throughput and impose latency penalties, is currently out of scope for OSACA.”

The LLVM Machine Code Analyzer (llvm-mca) [8] is a tool that predicts the performance of machine code based on a simulation using information that is available in the LLVM compiler [30]. It supports processors for which a scheduling model is available in LLVM. The tool does not model performance bottlenecks in the front end. It also does not model techniques such as micro/macro fusion or move elimination.

Renda et al. present DiffTune [11], which is an approach that replaces the microarchitecture-specific parameters of the x86 simulation model used by llvm-mca with parameters that are obtained automatically using machine learning.

Within the MAQAO [31] framework, two performance analysis tools have been proposed: CQA [9] and UFS [32]. The Code Quality Analyzer (CQA) is a tool that analyzes the performance of innermost loops. In addition to computing throughput predictions, it provides high-level code quality metrics like the vectorization ratio. CQA uses a front-end model that is more detailed than those of most other previous tools; however, it does not model the core of the execution engine “because of its complexity and lack of documentation.” UFS is a throughput predictor that uses a relatively detailed model of the back end of the Sandy Bridge microarchitecture, but only a very coarse-grained model of its front end. UFS exists only as a prototype that is not publicly available.

Ithemal [10] is a basic block throughput predictor that is based on a deep neural network. Unlike most of the other tools discussed in this section, it only predicts the throughput and provides no other insights into how the code is executed.

6.2 Microbenchmarking

nanoBench [13, 33] is a tool for evaluating small microbenchmarks on x86 systems using hardware performance counters. nanoBench is used for running the microbenchmarks for obtaining the latency, throughput, and port usage data that is available at uops.info [19].

Agner Fog [34] provides a measurement tool and a set of test scripts that generate microbenchmark to analyze various properties of microarchitectures. He maintains a set of tables

with instruction latencies, throughputs and micro-operation breakdowns [25], as well as a document with detailed descriptions of many recent microarchitectures [21].

PMEvo [26] is a framework by Ritter and Hack that can automatically infer port mappings based on measured execution times of short code sequences.

A related approach that also takes into account other limiting resources besides execution ports was recently proposed by Derumigny et al. [35].

7. CONCLUSIONS

We have developed a new simulator to predict the throughput of basic blocks. Our evaluation demonstrates that modeling microarchitectural details that were considered to be rather insignificant by previous work, is in fact crucial for accurate predictions.

Unlike recently proposed machine learning-based techniques, our approach is not based only on end-to-end measurements, which gives a higher confidence that our model is not overfitting to measurement errors. Our results show that training and evaluating predictors on measurements obtained with the same, potentially biased, measurement methodology may result in misleading conclusions.

We will release our simulator under an open-source license.

REFERENCES

- [1] *Intel Architecture Code Analyzer User's Guide*, Intel Corporation, 2017, Document Number: 321356-001US. [Online]. Available: <https://software.intel.com/content/dam/develop/external/us/en/documents/intel-architecture-code-analyzer-3-0-users-guide-157552.pdf>
- [2] J. Hammer, J. Eitzinger, G. Hager, and G. Wellein, "Kerncraft: A tool for analytic performance modeling of loop kernels," in *Tools for High Performance Computing 2016*. Springer International Publishing, 2017, pp. 1–22. [Online]. Available: https://doi.org/10.1007/978-3-319-56702-0_1
- [3] S. Williams, A. Waterman, and D. Patterson, "Roofline: An insightful visual performance model for multicore architectures," *Communications of the ACM*, vol. 52, no. 4, p. 65–76, Apr. 2009. [Online]. Available: <https://doi.org/10.1145/1498765.1498785>
- [4] H. Stengel, J. Treibig, G. Hager, and G. Wellein, "Quantifying performance bottlenecks of stencil computations using the execution-cache-memory model," in *Proceedings of the 29th ACM International Conference on Supercomputing*, ser. ICS '15. New York, NY, USA: Association for Computing Machinery, 2015, p. 207–216. [Online]. Available: <https://doi.org/10.1145/2751205.2751240>
- [5] A. Bhattacharyya, A. Sandulescu, M. Neugschwandtner, A. Sorniotti, B. Falsafi, M. Payer, and A. Kurmus, "SMoTherSpectre: Exploiting speculative execution through port contention," in *Proceedings of the 2019 ACM SIGSAC Conference on Computer and Communications Security*, ser. CCS '19. New York, NY, USA: ACM, 2019, pp. 785–800. [Online]. Available: <http://doi.acm.org/10.1145/3319535.3363194>
- [6] J. Laukemann, J. Hammer, J. Hofmann, G. Hager, and G. Wellein, "Automated instruction stream throughput prediction for Intel and AMD microarchitectures," in *IEEE/ACM Performance Modeling, Benchmarking and Simulation of High Performance Computer Systems (PMBS)*. Los Alamitos, CA, USA: IEEE Computer Society, Nov. 2018, pp. 121–131. [Online]. Available: <https://doi.org/10.1109/PMBS.2018.8641578>
- [7] J. Laukemann, J. Hammer, G. Hager, and G. Wellein, "Automatic throughput and critical path analysis of x86 and ARM assembly kernels," in *IEEE/ACM Performance Modeling, Benchmarking and Simulation of High Performance Computer Systems (PMBS)*, Nov. 2019. [Online]. Available: <https://doi.org/10.1109/PMBS49563.2019.00006>
- [8] "llvm-mca — LLVM machine code analyzer," 2021. [Online]. Available: <https://llvm.org/docs/CommandGuide/llvm-mca.html>
- [9] A. S. Charif-Rubial, E. Oseret, J. Noudouhouenou, W. Jalby, and G. Lartigue, "CQA: A code quality analyzer tool at binary level," in *21st International Conference on High Performance Computing (HiPC)*, Dec. 2014, pp. 1–10. [Online]. Available: <http://www.maqao.org/publications/papers/CQA.pdf>
- [10] C. Mendis, A. Renda, S. Amarasinghe, and M. Carbin, "Ithema: Accurate, portable and fast basic block throughput estimation using deep neural networks," in *Proceedings of the 36th International Conference on Machine Learning*, ser. Proceedings of Machine Learning Research, vol. 97. Long Beach, California, USA: PMLR, Jun. 2019, pp. 4505–4515. [Online]. Available: <http://proceedings.mlr.press/v97/mendis19a.html>
- [11] A. Renda, Y. Chen, C. Mendis, and M. Carbin, "DiffTune: Optimizing CPU simulator parameters with learned differentiable surrogates," in *53rd Annual IEEE/ACM International Symposium on Microarchitecture (MICRO)*, Oct. 2020, pp. 442–455. [Online]. Available: <https://doi.org/10.1109/MICRO50266.2020.00045>
- [12] Y. Chen, A. Brahmakshatriya, C. Mendis, A. Renda, E. Atkinson, O. Sykora, S. Amarasinghe, and M. Carbin, "BHive: A benchmark suite and measurement framework for validating x86-64 basic block performance models," in *2019 IEEE International Symposium on Workload Characterization (IISWC)*. IEEE, Nov. 2019. [Online]. Available: <http://groups.csail.mit.edu/commit/papers/19/ithema-measurement.pdf>
- [13] A. Abel and J. Reineke, "nanoBench: A low-overhead tool for running microbenchmarks on x86 systems," in *2020 IEEE International Symposium on Performance Analysis of Systems and Software (ISPASS)*, Aug. 2020. [Online]. Available: <https://doi.org/10.1109/ISPASS48437.2020.00014>
- [14] B. Falk, "Sushi Roll: A CPU research kernel with minimal noise for cycle-by-cycle micro-architectural introspection," Aug. 2019. [Online]. Available: https://gamazolabs.github.io/metrology/2019/08/19/sushi_roll.html
- [15] S. van Schaik, A. Milburn, S. Österlund, P. Frigo, G. Maisuradze, K. Razavi, H. Bos, and C. Giuffrida, "RIDL: Rogue in-flight data load," in *40th IEEE Symposium on Security and Privacy (SP)*, May 2019, pp. 88–105. [Online]. Available: <https://doi.org/10.1109/SP.2019.00087>
- [16] "Skylake (client) - Microarchitectures - Intel." [Online]. Available: [https://en.wikichip.org/wiki/intel/microarchitectures/skylake_\(client\)](https://en.wikichip.org/wiki/intel/microarchitectures/skylake_(client))
- [17] D. Kanter, "Intel's Haswell CPU microarchitecture," Nov. 2012. [Online]. Available: <https://www.realworldtech.com/haswell-cpu/2/>
- [18] *Intel 64 and IA-32 Architectures Optimization Reference Manual*, Intel Corporation, May 2020, Order Number: 248966-043. [Online]. Available: <https://software.intel.com/content/dam/develop/public/us/en/documents/64-ia-32-architectures-optimization-manual.pdf>
- [19] A. Abel and J. Reineke, "uops.info: Characterizing latency, throughput, and port usage of instructions on Intel microarchitectures," in *Proceedings of the Twenty-Fourth International Conference on Architectural Support for Programming Languages and Operating Systems (ASPLOS)*, Providence, RI, USA, April 13-17, 2019, ser. ASPLOS '19. ACM, 2019, pp. 673–686. [Online]. Available: <http://doi.acm.org/10.1145/3297858.3304062>
- [20] I. Cutress, "The Intel Skylake-X review: Core i9 7900X, i7 7820X and i7 7800X tested," Jun. 2017. [Online]. Available: <https://www.anandtech.com/show/11550/the-intel-skylakex-review-core-i9-7900x-i7-7820x-and-i7-7800x-tested/3>
- [21] A. Fog, "The microarchitecture of Intel, AMD, and VIA CPUs," Technical University of Denmark, Mar. 2021. [Online]. Available: <https://www.agner.org/optimize/microarchitecture.pdf>
- [22] "Mitigations for jump conditional code erratum," Intel Corporation, Nov. 2019, Document Number: 341810-001. [Online]. Available: <https://www.intel.com/content/dam/support/us/en/documents/processors/mitigations-jump-conditional-code-erratum.pdf>
- [23] "6th generation Intel processor family — Specification update," Intel Corporation, Dec. 2020, Document Number: 332689-027. [Online]. Available: <https://www.intel.com/content/www/us/en/processors/core/desktop-6th-gen-core-family-spec-update.html>
- [24] "10th generation Intel Core processor families — Specification update," Intel Corporation, Mar. 2021, Document Number: 341079-009. [Online]. Available: <https://www.intel.de/content/www/de/de/products/docs/processors/core/10th-gen-core-families-specification-update.html>

- [25] A. Fog, "Instruction tables: Lists of instruction latencies, throughputs and micro-operation breakdowns for Intel, AMD and VIA CPUs," Technical University of Denmark, Mar. 2021. [Online]. Available: http://www.agner.org/optimize/instruction_tables.pdf
- [26] F. Ritter and S. Hack, "PMEvo: Portable inference of port mappings for out-of-order processors by evolutionary optimization," in *Proceedings of the 41st ACM SIGPLAN Conference on Programming Language Design and Implementation*, ser. PLDI 2020. New York, NY, USA: Association for Computing Machinery, 2020, p. 608–622. [Online]. Available: <https://doi.org/10.1145/3385412.3385995>
- [27] Z. H. Jiang and Y. Fei, "A novel cache bank timing attack," in *Proceedings of the 36th International Conference on Computer-Aided Design*, ser. ICCAD '17. IEEE Press, Nov. 2017, p. 139–146. [Online]. Available: <https://dl.acm.org/doi/abs/10.5555/3199700.3199719>
- [28] J. D. McCalpin, "Comments on timing short code sections on Intel processors," Jul. 2018. [Online]. Available: <https://sites.utexas.edu/jdm4372/2018/07/23/comments-on-timing-short-code-sections-on-intel-processors/>
- [29] M. G. Kendall, "A new measure of rank correlation," *Biometrika*, vol. 30, no. 1/2, pp. 81–93, 1938. [Online]. Available: <https://doi.org/10.2307/2332226>
- [30] C. Lattner and V. Adve, "LLVM: A compilation framework for lifelong program analysis & transformation," in *Proceedings of the International Symposium on Code Generation and Optimization: Feedback-directed and Runtime Optimization*, ser. CGO '04. Washington, DC, USA: IEEE Computer Society, 2004, pp. 75–86. [Online]. Available: <http://dl.acm.org/citation.cfm?id=977395.977673>
- [31] "MAQAO (modular assembly quality analyzer and optimizer)." [Online]. Available: <http://www.maqao.org>
- [32] V. Palomares, D. C. Wong, D. J. Kuck, and W. Jalby, "Evaluating out-of-order engine limitations using uop flow simulation," in *Tools for High Performance Computing 2015*. Springer International Publishing, 2016, pp. 161–181. [Online]. Available: https://dx.doi.org/10.1007/978-3-319-39589-0_13
- [33] A. Abel, "Automatic generation of models of microarchitectures," Ph.D. dissertation, Universität des Saarlandes, Jun. 2020. [Online]. Available: <https://d-nb.info/1212853466/34>
- [34] A. Fog, "Test programs for measuring clock cycles and performance monitoring." [Online]. Available: <https://www.agner.org/optimize/>
- [35] N. Derumigny, F. Gruber, T. Bastian, C. Guillon, L.-N. Pouchet, and F. Rastello, "From micro-OPs to abstract resources: constructing a simpler CPU performance model through microbenchmarking," Jan. 2021. [Online]. Available: <https://arxiv.org/abs/2012.11473>

APPENDIX

A. HEATMAPS FOR ICE LAKE

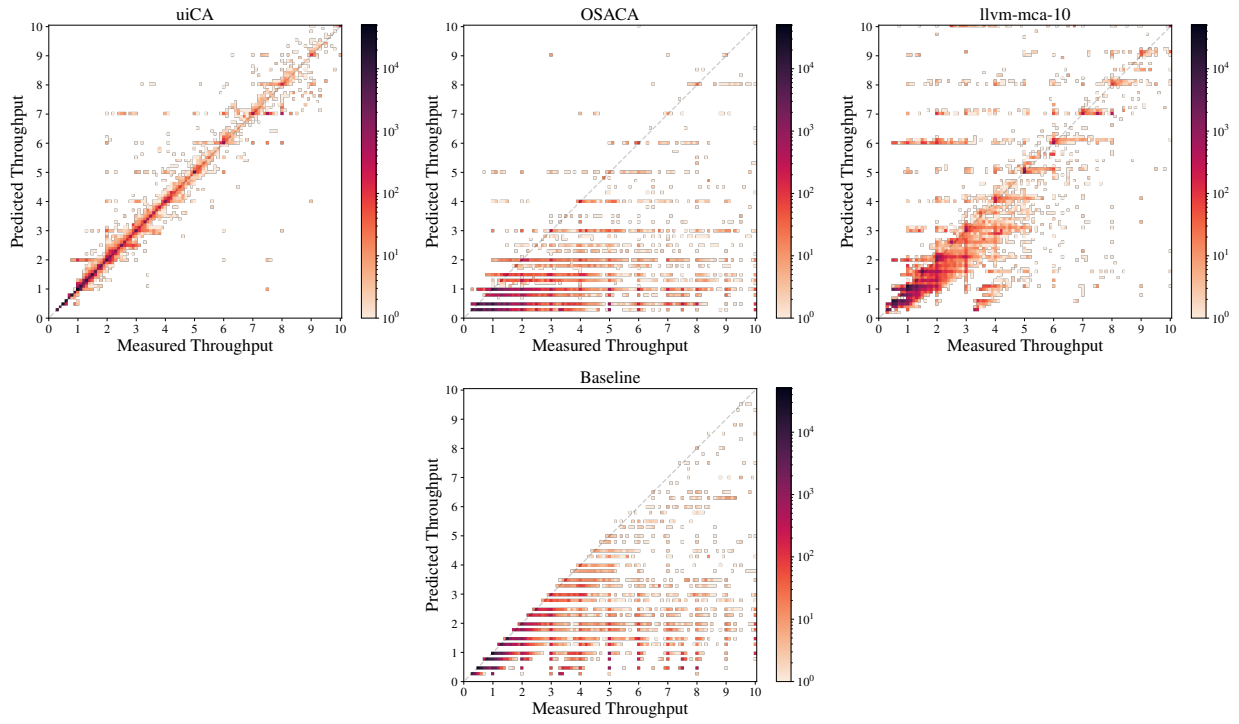


Figure 2: Heatmaps for $BHive_U$ for basic blocks with a measured throughput of less than 10 cycles/iteration on Ice Lake

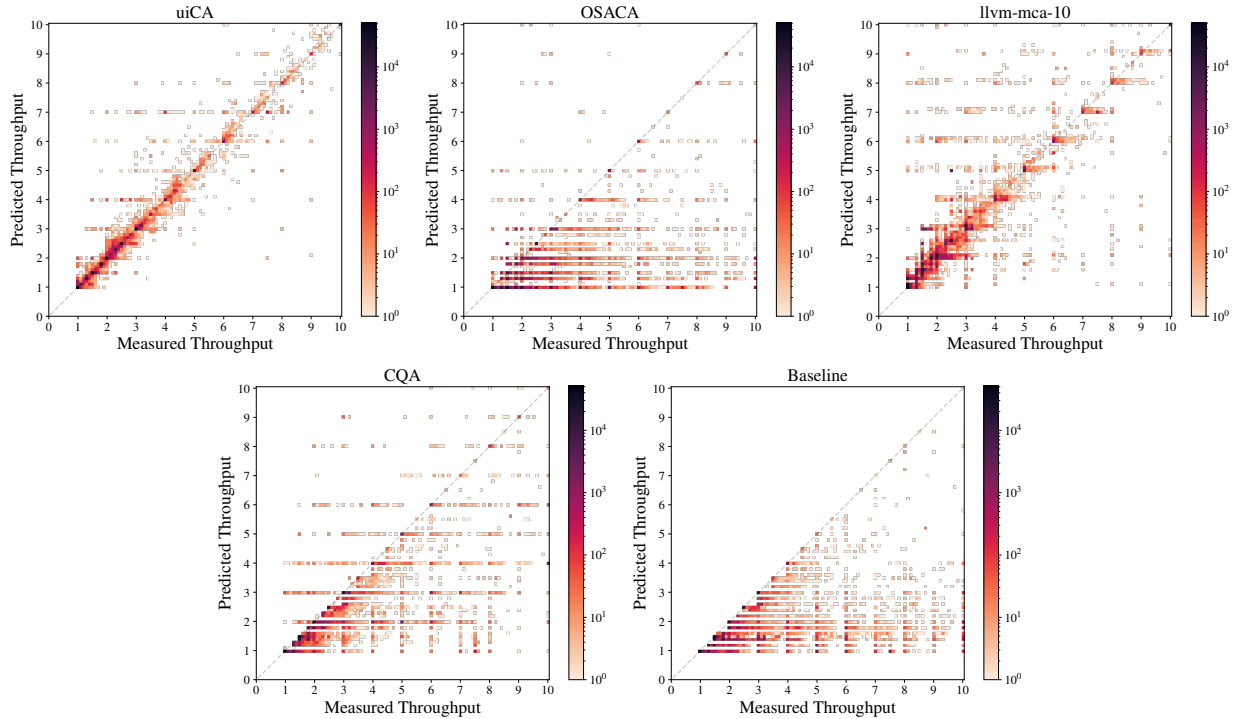


Figure 3: Heatmaps for $BHive_L$ for basic blocks with a measured throughput of less than 10 cycles/iteration on Ice Lake

B. HEATMAPS FOR SKYLAKE

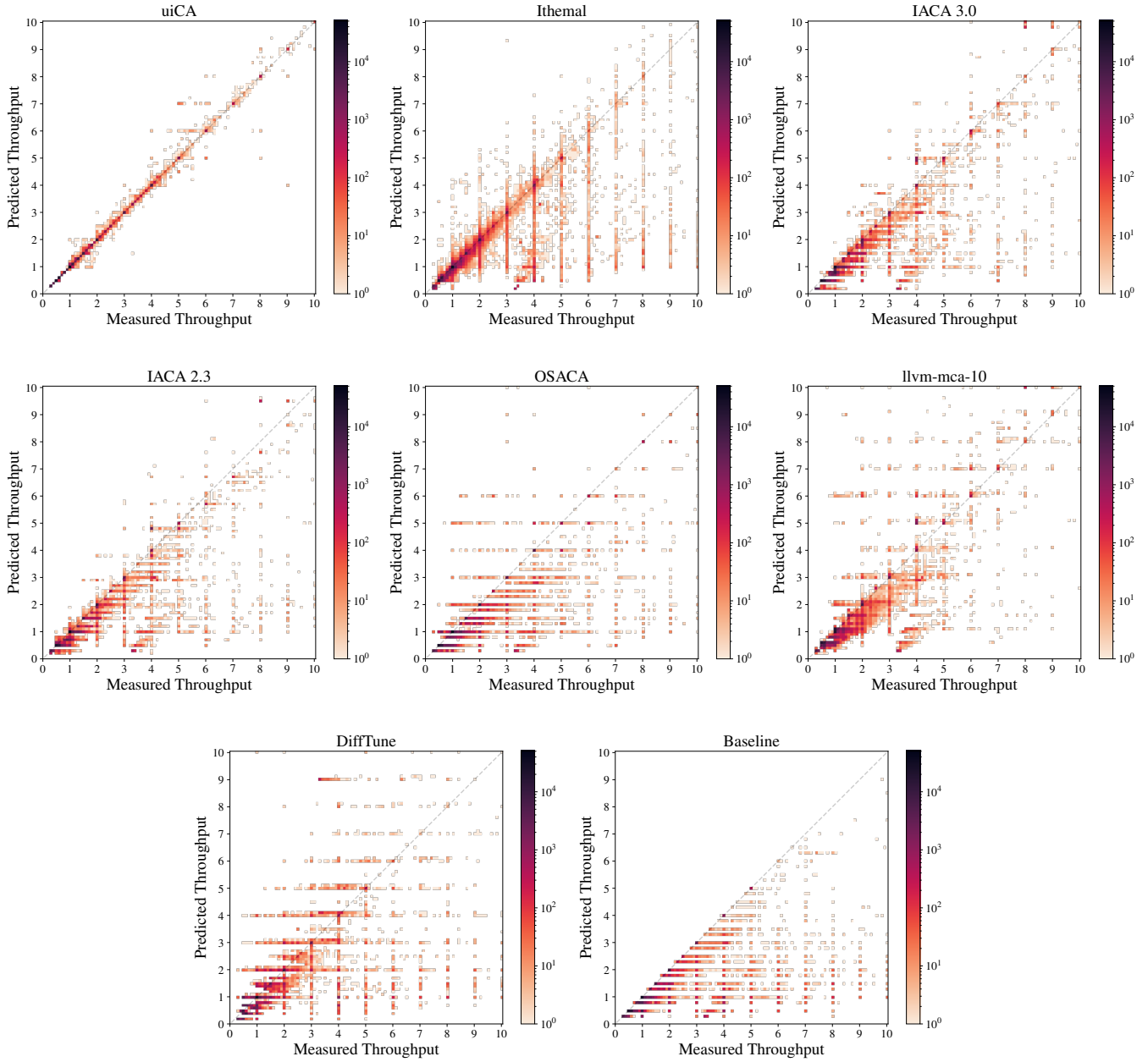


Figure 4: Heatmaps for $BHive_U$ for basic blocks with a measured throughput of less than 10 cycles/iteration on Skylake

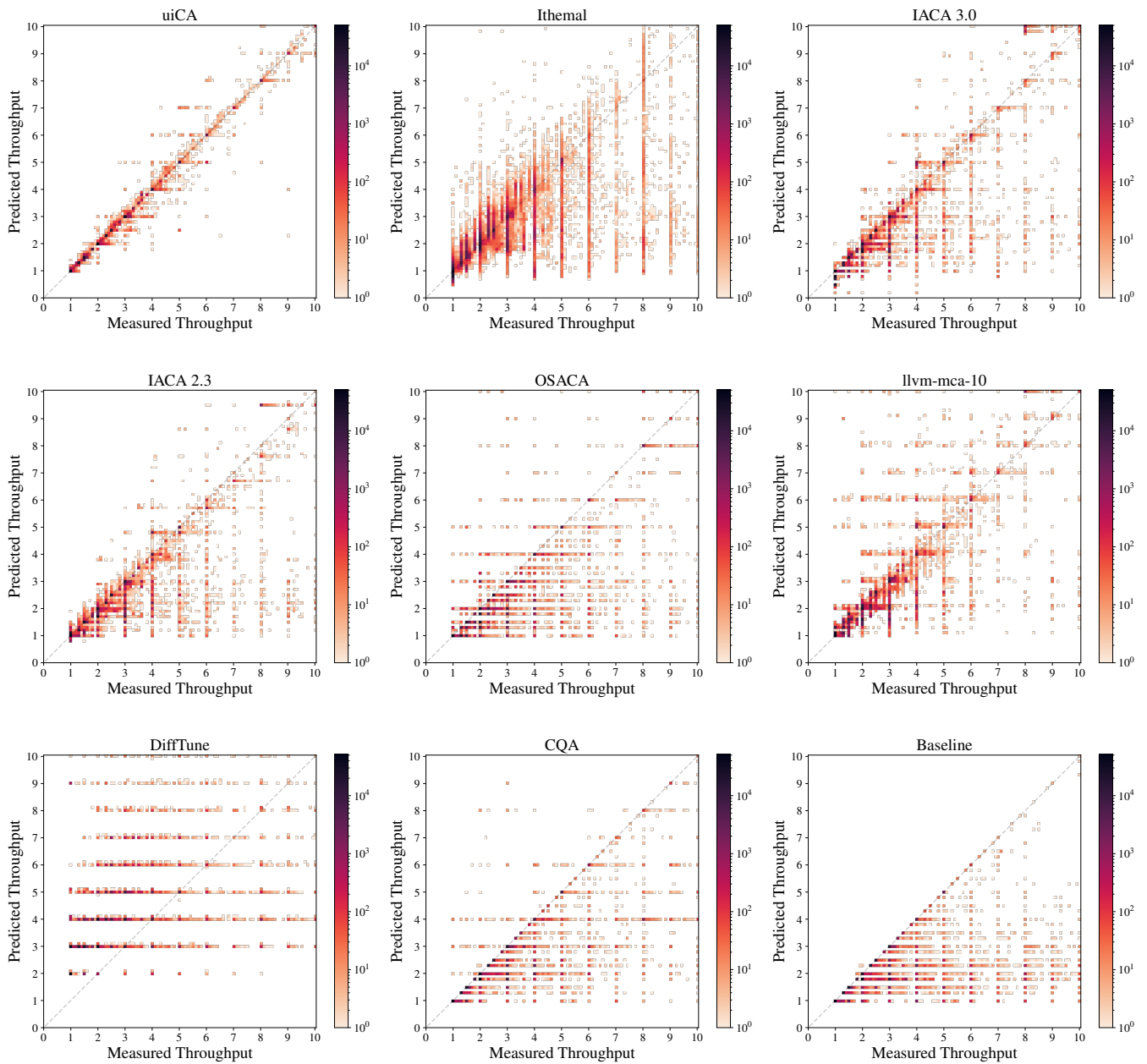


Figure 5: Heatmaps for $BHive_L$ for basic blocks with a measured throughput of less than 10 cycles/iteration on Skylake

C. HEATMAPS FOR HASWELL

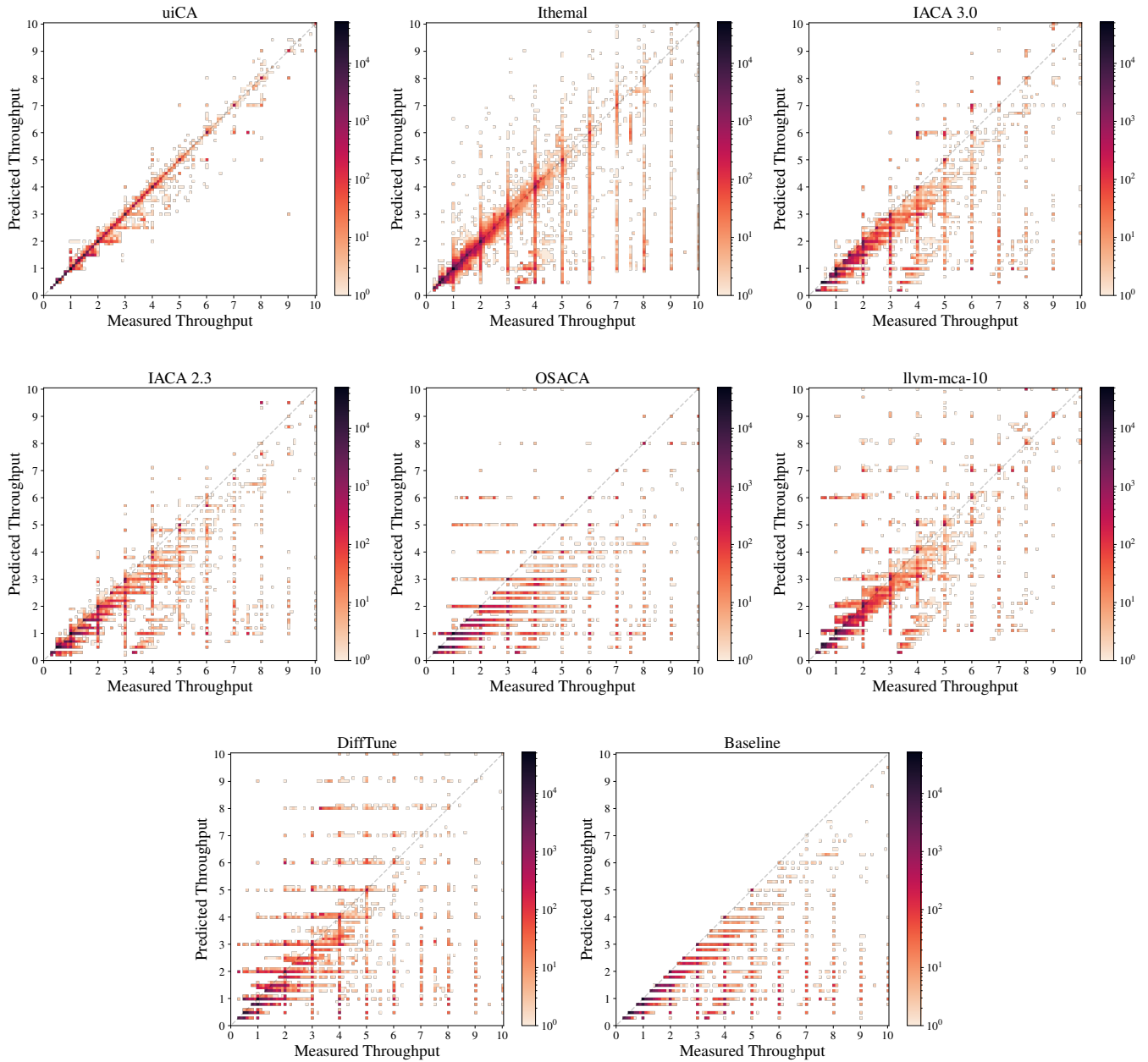


Figure 6: Heatmaps for $BHive_U$ for basic blocks with a measured throughput of less than 10 cycles/iteration on Haswell

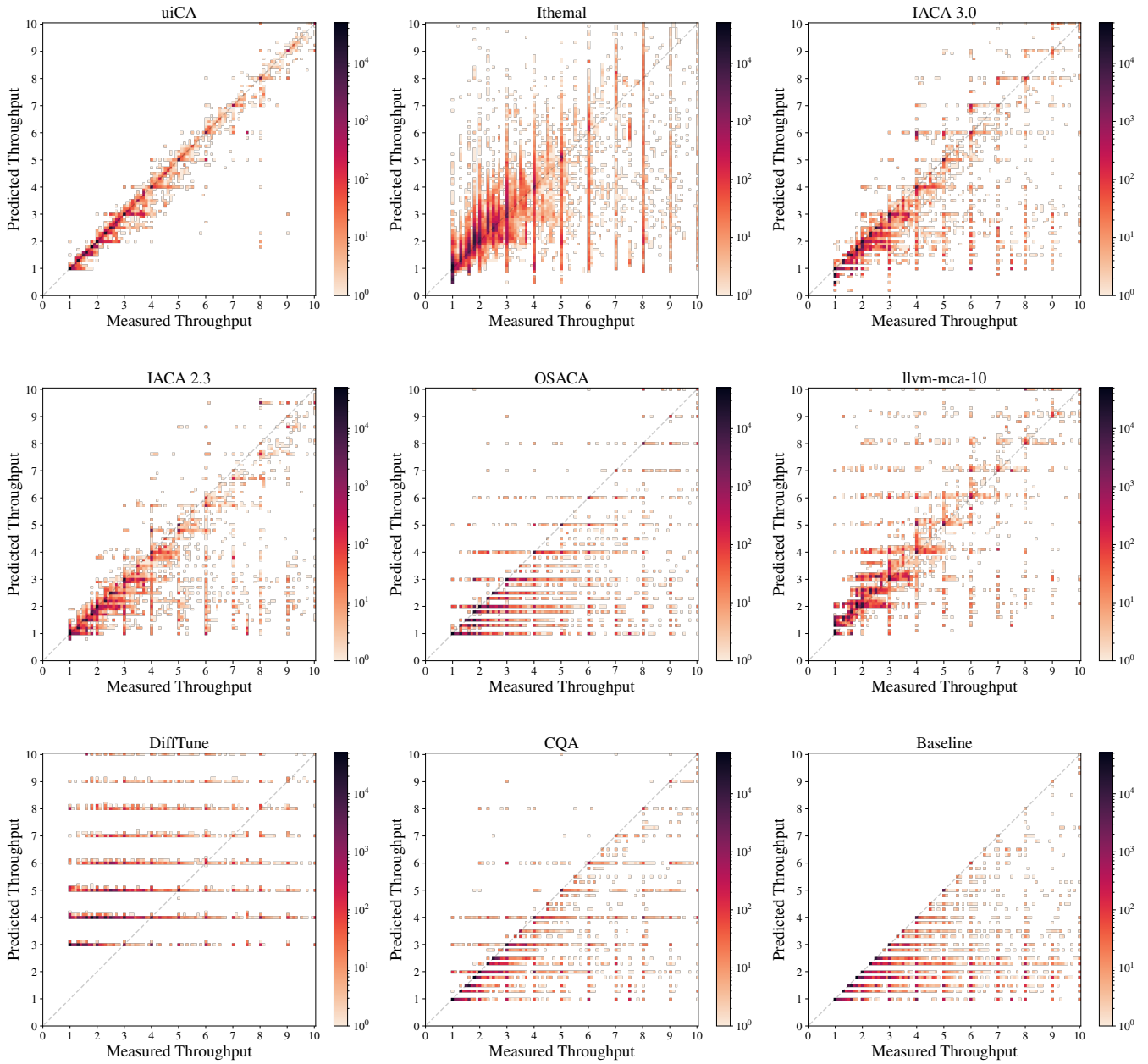


Figure 7: Heatmaps for $BHive_L$ for basic blocks with a measured throughput of less than 10 cycles/iteration on Haswell

D. HEATMAPS FOR IVY BRIDGE

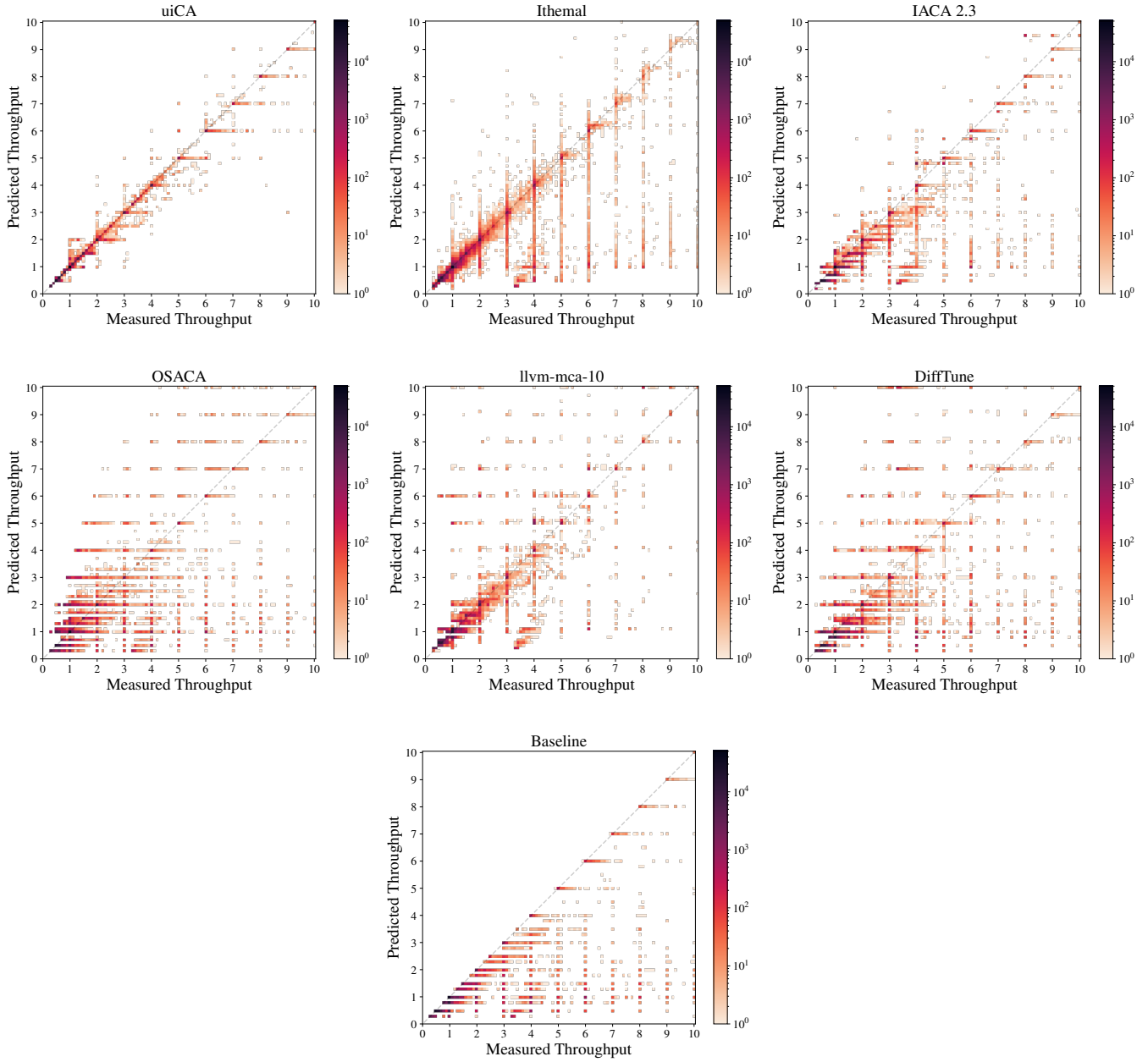


Figure 8: Heatmaps for $BHive_U$ for basic blocks with a measured throughput of less than 10 cycles/iteration on Ivy Bridge

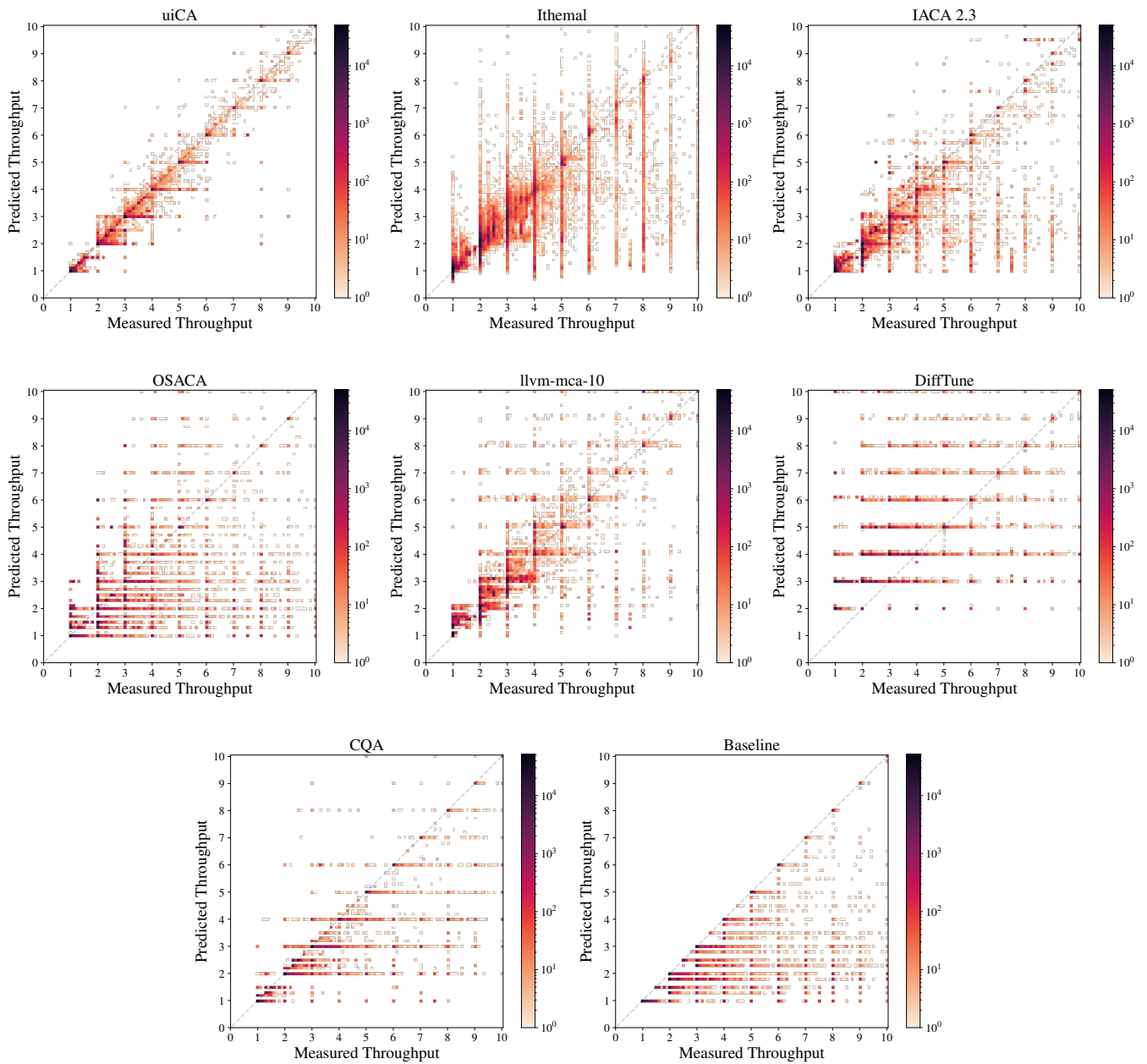


Figure 9: Heatmaps for $BHive_L$ for basic blocks with a measured throughput of less than 10 cycles/iteration on Ivy Bridge